Steel and Composite Structures, *Vol. 32, No. 3 (2019) 411-422*
DOI: https://doi.org/10.12989/scs.2019.32.3.411

Shear behavior of short square tubed steel reinforced concrete columns with high-strength concrete

Xiang Li [1,2a], Xuhong Zhou [1,2b], Jiepeng Liu [1,2c] and Xuanding Wang [*1,2]

[1] *School of Civil Engineering, Chongqing University, Chongqing 400045, China*
[2] *Key Laboratory of New Technology for Construction of Cities in Mountain Area (Chongqing University), Ministry of Education, Chongqing 400045, China*

(*Received April 9, 2019, Revised June 11, 2019, Accepted June 21, 2019*)

Abstract. Six shear-critical square tubed steel reinforced concrete (TSRC) columns using the high-strength concrete ($f_{cu,150}$ = 86.6 MPa) were tested under constant axial and lateral cyclic loads. The height-to-depth ratio of the short column specimens was specified as 2.6, and the axial load ratio and the number of shear studs on the steel shape were considered as two main parameters. The shear failure mode of short square TSRC columns was observed from the test. The steel tube with diagonal stiffener plates provided effective confinement to the concrete core, while welding shear studs on the steel section appeared not significantly enhancing the seismic behavior of short square TRSC columns. Specimens with higher axial load ratio showed higher lateral stiffness and shear strength but worse ductility. A modified ACI design method is proposed to calculate the nominal shear strength, which agrees well with the test database containing ten short square TSRC columns with shear failure mode from this study and other related literature.

Keywords: tubed steel reinforced concrete (TSRC) column; square cross-section; shear studs; high-strength concrete (HSC); seismic test; shear failure mode

1. Introduction

As a primary type of composite columns, steel reinforced concrete (SRC) columns are widely used in high-rise buildings due to their advantages including: great stiffness, not prone to buckle locally, cost-effectiveness, high load capacity, and quick construction (Ky *et al*. 2015, Fumiya and Masayuki 2001, An *et al*. 2018, Lu *et al*. 2014). The concrete also provides fire resistance to the steel shape (Piquer and Hernández-Figueirido 2016). However, two obvious limitations for engineers to use SRC in structural design existed: (1) The insufficiency in effective confinement supplied by stirrups may lead to brittle failure for columns under a high axial load (Chen *et al*. 2016, Wang *et al*. 2016); and (2) The construction process of the rebar and the steel shape in the beam-column connection is complex (El-Tawil and Deierlein 1999). Recently, high-strength concrete (HSC) has gained increasing attention due to various reasons, such as increasing available floor area and promoting environmental sustainability. However, the brittleness of HSC makes it inapplicable for the SRC columns without sufficient confinement (Zhou and Liu 2010, Choi *et al*. 2012).

To provide more effective lateral confinement to the concrete core and simplify the construction of traditional SRC columns, a new type of composite column called tubed steel reinforced concrete (TSRC) was proposed by Zhou and Liu (2010). In this system, the longitudinal and transverse reinforcing bars are removed and the concrete core with the inner steel shape is confined by an outer thin-walled steel tube which is stopped at the beam-column joints to avoid carrying direct axial loads and maximize the confinement. Compared to SRC column, the steel tube provides more effective confinement which enhances the strength and ductility of the inner concrete and prevents the concrete cover from spalling off. Besides, the beam-column joints of this new type of column are much easier to construct since the steel tube discontinues at the column ends (Zhang *et al*. 2018).

The most important feature of TSRC is the confinement from the disconnected steel tube. Such composite member had been investigated by Gardner and Jacobson (1967) as a contrasting CFST column specimen where only the concrete core was loaded. Some similar investigations were carried out by Johansson and Gylltoft (2002) and Fam *et al*. (2004). Their studies indicated that the end loading condition had little influence on the axial strength of CFST columns due to the friction between the concrete and the steel tube, while the development of stresses in the steel tube was quite different. To further enhance the tube confinement to the concrete core, O'shear and Bridge (2000) focused on the behavior of unbonded tubed concrete columns where antifriction material was applied to the inner surface of the steel tube to maximize the confinement effect. Tomii *et al*. (1985) first introduced the tubed

*Corresponding author, Ph.D.,
E-mail: wangxuanding@cqu.edu.cn
[a] Ph.D. Student
[b] Ph.D., Professor
[c] Ph.D., Professor

ISSN: 1229-9367 (Print), 1598-6233 (Online)

concrete column concept into the traditional reinforced concrete field with the initial idea of improving shear strength for the edge columns of shear walls and the short columns restrained by spandrel walls. Since then, performances on tubed concrete members have been extensively studied with promising results (McAteer *et al.* 2004, Han *et al.* 2005). Recently, Xiong *et al.* (2017) experimentally studied the tubed concrete members with high- and ultra-high-strength materials and proposed the design recommendations. Nematzadeh *et al.* (2017) revealed that the effect of the active and passive confinement on modulus of steel tube-confined concrete stub columns was different. Zhao *et al.* (2018) investigated the loading path effect on the compressive strength of confined concrete in concrete-filled steel tube (CFT) columns and found that the confinement effect was influenced not only by the ultimate confining stress but also by the loading path. Guo *et al.* (2019) experimentally studied the axial behavior of stub column which was confined by stainless steel tube. It was indicated that the axial stress of steel tube contributed to the load-carrying capacity. Disconnected steel tube can also notably enhance the uniaxial strength and ductility of short column using ultra high performance concrete (UHPC) from test results of Le Hoang *et al.* (2019). For the post-fire behavior of tubed concrete members, Yang *et al.* (2015) proposed a simplified design method for residual capacity of reinforced concrete confined by circular steel tube after ISO 834 standard fire exposure. However, as a new kind of tubed concrete members, the study on the TSRC column is relatively limited. Compared to SRC columns, the seismic behavior of TSRC columns with circular and square cross-sections exhibited higher shear strength, plastic deformation capacity, ductility, and energy dissipating capacity according to the test results of Zhou and Liu (2010) and Liu *et al.* (2011). In their tests, longitudinal bond cracks appeared between the concrete and the flanges of steel shape. Thus, they recommended welding the shear studs on the steel shape to prevent bond failure.

To sum up, the TSRC column has a good application prospect according to the previous studies. There, however, exists a knowledge gap related to this type of columns especially with regards to short columns with HSC failed in shear mode. Moreover, the effect of shear studs on the seismic behavior of shear-critical TSRC columns has not been studied yet. In this study, an experimental investigation of six short square TSRC columns (height-to-depth ratio = 2.6) using HSC is conducted. The key parameters considered are axial load ratio (0.3, 0.5) and the number of shear studs on the steel shape (0, 3, 5 and 7). A modified ACI design method (2011) for HSC is adopted to calculate the shear strength of square TSRC column, which results in a close agreement with the measured shear strength.

2. Experimental program

2.1 Specimen design

In order to investigate the seismic behavior of short square TSRC columns failed in shear mode, columns with a height-to-depth ratio of 2.6 were tested under constant axial load and cyclic horizontal forces. Two main parameters which may influence the seismic behavior of columns were studied: the axial load ratio, and the number of shear studs on the steel shape. The axial load ratio can be calculated by $n = N/(A_c f_c + A_f f_f + A_w f_w)$ where the A_c, A_f, and A_w are the areas of concrete, steel flanges and steel web, respectively, f_c is the compressive strength of the concrete, and f_f and f_w are the average yield stress of the steel flange and the steel web, respectively. Note that to study the effect of the D/t ratio on seismic behavior under the same steel tube strength, the wall-thickness of the steel tube of all test specimens keep unchanged, while enlarging the overall dimension for the specimen with higher D/t ratio (i.e., STSRC-270-3-7). Details of the specimens are shown in Table 1, where H is the column height, D is the width of cross section, t is the wall-thickness of the steel tube, h_s and b_s are respectively the height and width of the steel shape, t_f and t_w are respectively the thickness of steel flange and steel web, and N_s is the number of shear studs on each steel shape flange. An example of the test specimen identification system is as follows: STSRC-220-5-5, where STSRC represents a square tubed steel reinforced-concrete column, the next digit number '220' denotes D = 220 mm, the following digit '5' accounts for the axial load ratio n of 0.5, the last one '5' denotes the number of shear studs on each flange of the steel shape is 5.

2.2 Specimen construction

Fig. 1 shows the geometry of typical test specimens. To prevent local buckling and enhance the confinement effect of the square steel tube, four diagonal stiffened plates of 220 mm × 104 mm × 2 mm were welded on adjacent sides

Table 1 Details of the test specimens

Specimens	H (mm)	D (mm)	t (mm)	D/t	h_s (mm)	b_s (mm)	t_f (mm)	t_w (mm)	N_s	N (kN)	n
STSRC-220-5-0	572	220	2	110	125	125	9	6	0	2180	0.5
STSRC-220-3-3	572	220	2	110	125	125	9	6	3	1300	0.3
STSRC-220-5-3	572	220	2	110	125	125	9	6	3	2180	0.5
STSRC-220-3-5	572	220	2	110	125	125	9	6	5	1300	0.3
STSRC-220-5-5	572	220	2	110	125	125	9	6	5	2180	0.5
STSRC-270-3-7	702	270	2	135	175	165	9	6	7	1925	0.3

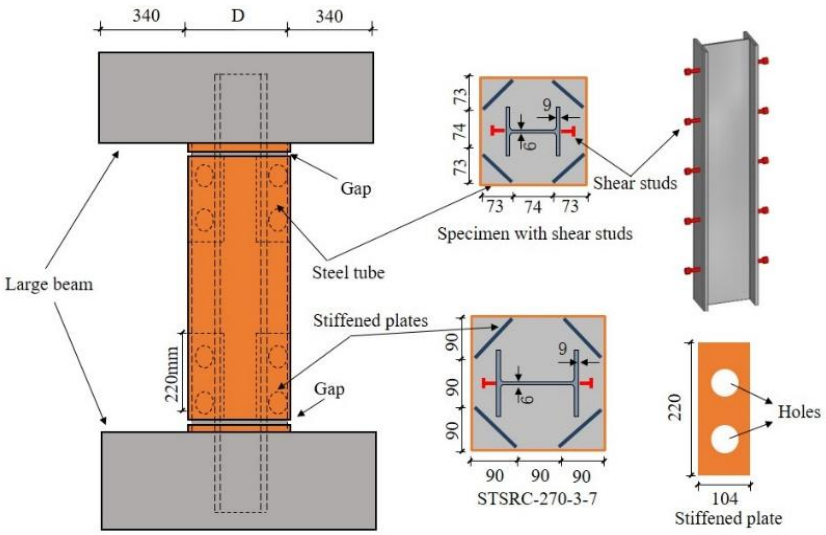

Fig. 1 The geometry of test specimens

of the square steel tube. Note that the holes on the stiffened plates aim to facilitate the process of concrete pouring. The shear studs were welded evenly along the steel shape flange. All specimens were cast vertically using the same batch concrete. Each specimen consisted of two 500 × 576.5 × 900 mm large beams fixed at the top and bottom of the column to generate accurate fixed boundary conditions. After the cast concrete becoming hardened the steel tube was cut off at 20 mm away from each column end to ensure the steel tube not directly sharing the axial load.

2.3 Material properties

To evaluate the concrete compressive strength ($f_{cu,150}$), a total of twelve standard concrete cubes of 150 mm × 150 mm × 150 mm were cast. These cubes were conforming to the Chinese concrete code (GB50010-2010) (2011) and were tested at 28 days and during the test days. The elastic modulus of concrete (E_c) was determined by testing three concrete prisms of 150 mm × 150 mm × 300 mm. The equivalent value of cylinder strength f_c was developed from conversion factors specified in CEB-FIP Model Code 1990 (1993). Table 2 listed the detailed concrete properties.

The steel material parameters of steel shape and square steel tube were determined by testing tensile coupons made using the same batch steel plates according to the Chinese Standard GB/T228-2010 (2010). The key parameters such as average yield strength, average ultimate strength and average elastic modulus are presented in Table 3.

Table 2 Average concrete properties

Testing time	150 mm Cube strength $f_{cu,150}$ (MPa)	Average compressive strength f_c(MPa)	Elastic modulus E_c (GPa)
28 days	79.5	64.42	-
The test day	86.6	70.35	44

2.4 Testing and instrumentation

The test rig used in this study is shown in Fig. 2, which mainly consists of a L-shape loading frame and a moveable truss system. The foundation large beam of the specimen was fully fixed on the ground using high-strength steel strands, whereas the top large beam of the specimen was attached to L-shape loading frame in order to make the horizontal movement with no rotation. Each specimen was tested by applying the constant vertical compression load first using a 2500 kN MTS hydraulic jack. The lateral force, simulating the seismic loading, was then cyclically applied using a 1000 kN capacity MTS actuator. The loading program of the specimen was shown in Fig. 3. During the load control stage, only one loading cycle was applied with an increment of 30kN. After the specimen was yielded, the displacement control method was used. Two repetitive loading cycles were applied for each of the peak lateral cyclic displacements, $\Delta = \Delta_y, 2\Delta_y, 3\Delta_y\ldots$ etc., where Δ_y is the yielding displacement of the column. The test ended when the lateral load resisting capacity dropped by more than 20% of the maximum lateral load.

Fig. 4 shows the instrumentation layout for the specimens. Two linear variable differential transducers (LVDTs) fixed with the outstretched rod were used to measure the relative horizontal displacements between the top and bottom large beams of the columns. To record

Table 3 Average steel properties

Steel type	Average yield strength (MPa)	Average ultimate strength (MPa)	Average elastic modulus (GPa)
Steel tube	245.0	374.0	186
Flange of steel shape	384.1	520.1	184
Web of steel shape	404.4	518.6	184

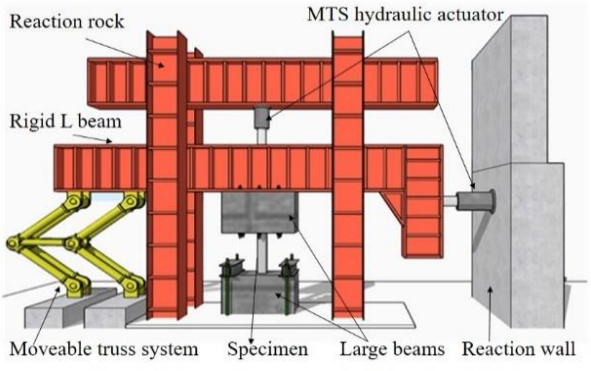

(a) Sketch

(b) Photo

Fig. 2 Test setup

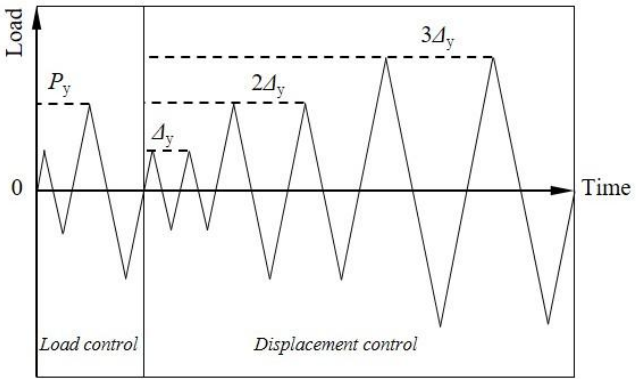

Fig. 3 Lateral loading program

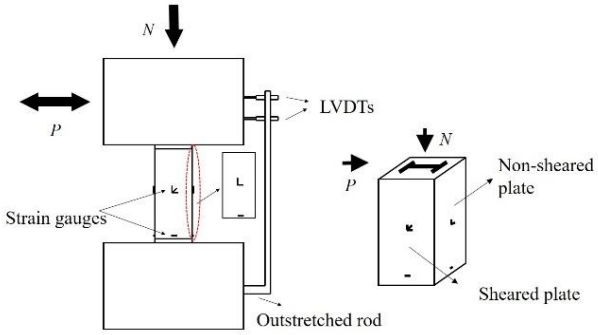

(a) Sketch

(b) Photo

Fig. 4 The instrumentation layout

the strain variation of steel tube, electrical resistance strain gauges were attached to the outer surface of steel tube at mid-height and bottom of the column. The layout of strain gauges on the sheared plate and non-sheared plate is different, as shown in Fig. 4.

3. Test results and discussions

3.1 Failure modes

Fig. 5 shows the failure modes of the tested short square TSRC columns. Slight outward local buckling of steel tube was observed in all test specimens at both the column ends. After the tests, the steel tubes of all specimens were removed to observe the damage of the enclosed concrete. For specimens with a cross-sectional side width of 220 mm, the concrete cover at both the column ends was seriously crashed and obvious diagonal shear cracks were found in the middle region of the column. Bond cracks were also found in specimens with shear studs and those without, showing that shear studs did not effectively prevent the development of bond cracks between the flanges of the steel shape and concrete. The failure mode of these specimens can be characterized as a combination of bond and shear

(a) STSRC-220-5-0 (b) STSRC-220-3-3

(c) STSRC-220-5-3 (d) STSRC-220-3-5

(e) STSRC-220-5-5 (f) STSRC-270-3-7

Fig. 5 Failure modes of specimens

failure. However, compared with the previous study of the authors (Zhou and Liu 2010) where the splitting failure happened between the steel shape and concrete (Fig. 6), in this study the development of bond cracks was alleviated and the splitting failure was effectively avoided due to the enhancement of stiffeners on the tube confinement. Therefore, compared to using shear studs on steel shape, lateral confinement was crucial to the co-work performance between the steel shape and concrete, especially in the case of large deformation.

The failure mode of specimen STSRC-270-3-7 is different from other specimens, as presented in Fig. 5(f). That is, no obvious bond or shear cracks were found in this specimen and the concrete core maintained good integrity with only few vertical and horizontal cracks at the bottom end. This phenomenon may be caused by a premature failure of the top large beam (Fig. 5(f)). As such, the fixed boundary condition at the top of the column cannot be achieved, resulting in an increase of the column effective height and changing the failure mode from shear failure to

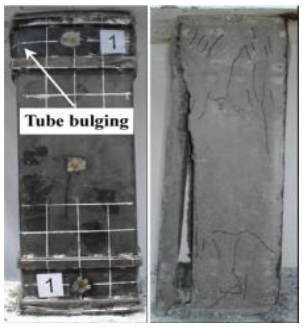

Fig. 6 Splitting failure between the steel shape and concrete in a previous study (Zhou and Liu 2010)

flexural failure.

3.2 Lateral load versus displacement hysteretic curves

The lateral load-displacement (*P*-*u*) hysteretic curves of test specimens are shown in Fig. 7. Note that the hysteretic curve of specimen STSRC-220-5-3 is incomplete because of an accident of the test frame. The characteristics of the hysteretic curves are summarized as follows.

Compared to the specimens with lower axial load ratio (e.g., STSRC-220-3-3 and STSRC-220-3-5), the specimens with higher axial load ratio (e.g., STSRC-220-5-0, STSRC-220-5-3 and STSRC-220-5-5) generally had higher lateral shear resistances. Taking Specimens STSRC-220-3-5 and STSRC-220-5-5 as examples, the peak lateral load increased by approximately 12% as the axial load ratio increased from 0.3 to 0.5. However, higher axial load ratio may result in a worse energy dissipation capacity of short square TSRC columns, as observed by narrow hysteretic loops arising from rapidly decreasing lateral resistance at relatively small drift. It appeared that the parameter of shear stud was unable to improve the hysteretic curves of square TSRC columns to gain a better seismic performance due to its limited ability to prevent bond and shear failure (Xue *et al*. 2012) compared with outer thin-walled steel tube, some specimens (e.g., STSRC-220-5-5) with more shear studs even had a worse ductility. Pinching effect can be obviously

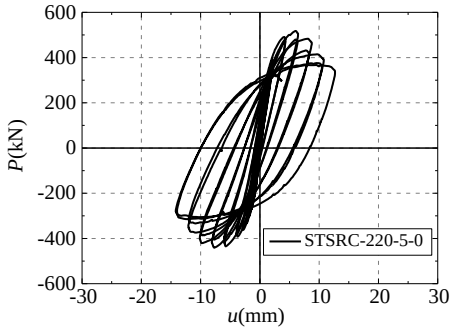

(a) STSRC-220-5-0

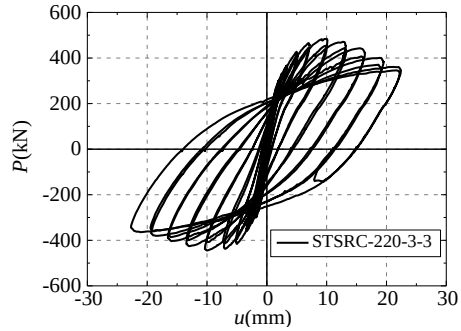

(b) STSRC-220-3-3

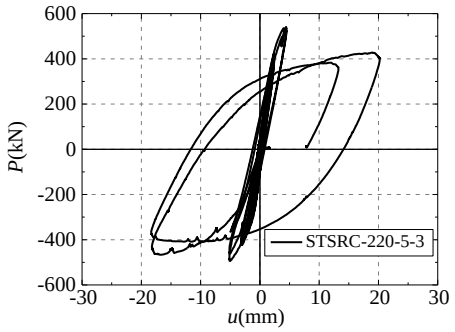

(c) STSRC-220-5-3

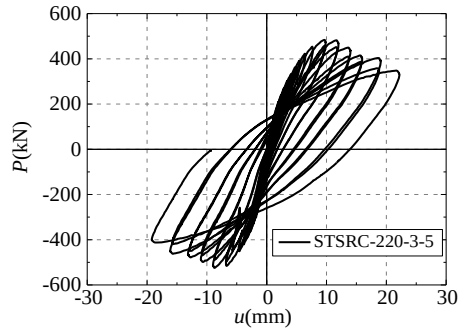

(d) STSRC-220-3-5

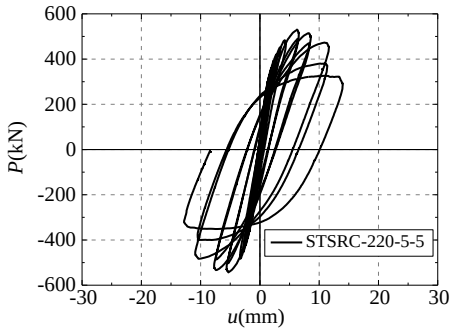

(e) STSRC-220-5-5

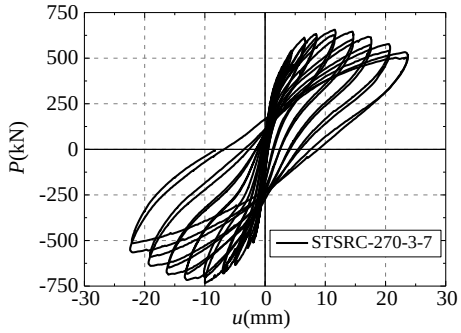

(f) STSRC-270-3-7

Fig. 7 Load-displacement hysteretic curves

Table 4 Mechanical parameters of the specimens

Specimen	P_y (kN)	Δ_y (mm)	P_u (kN)	Δ_u (mm)	$P_{0.85}$ (kN)	$\Delta_{0.85}$ (mm)	μ	φ
STSRC-220-5-0	450	2.9	518	6.0	500	9.1	3.21	1.9%
STSRC-220-3-3	427	7.6	484	10.0	411	17.9	3.55	3.1%
STSRC-220-5-3	485	3.0	541	4.4	460	10.5	3.50	2.6%
STSRC-220-3-5	418	6.2	484	9.6	411	15.7	2.53	2.7%
STSRC-220-5-5	472	3.1	544	5.3	462	12.0	3.87	2.1%
STSRC-270-3-7	620	4.6	733	10.0	623	21.9	4.26	3.1%

found in the hysteretic curve of STSRC-270-3-7 due to the flexural failure mode. While for the specimens in shear failure mode (e.g., specimens with a cross-sectional side width of 220 mm), the pinching effect is not obvious. Energy dissipation capacity for specimens failed in shear mode seem to be higher within the parameters considered in this test.

3.3 Envelop curves analysis

The envelops of the cyclic curves are shown in Fig. 8 and some key properties or factors of the curves were obtained, including the yield load and displacement (i.e., P_y and Δ_y), the peak load and displacement (i.e., P_u and Δ_u), the ultimate load and displacement as the lateral resistance reducing to 85% of the peak load (i.e., $P_{0.85}$ and $\Delta_{0.85}$), the ductility ratio μ, and the ultimate drift ratio φ, as listed in Table 4. Note that μ and φ are respectively determined by Eqs. (1) and (2) to reflect the ductility and plastic deformation ability of the specimens.

$$\mu=\frac{\Delta_{0.85}}{\Delta_y} \tag{1}$$

$$\varphi=\frac{\Delta_{0.85}}{L}\times 100\% \tag{2}$$

For the specimens with the same axial load ratio but different number of shear studs on the steel shape, the envelop curves were almost same. Taking the representative specimens, STSRC-220-5-0 and STSRC-220-5-5 for elaboration, as the number of shear studs increased from 0 to 5, the peak lateral load P_u increased by 5% and φ increases by 9% approximately. Thus, it can be concluded that the improvement of the peak lateral load and ultimate story drift ratio of the specimens by welding the shear studs on the steel shape was not remarkable.

To investigate the effect of axial load ratio on the behavior of short square TSRC columns, typical specimens STSRC-220-3-5 and STSRC-220-5-5 were compared as shown in Fig. 8(c). With the increase of axial load ratio, the

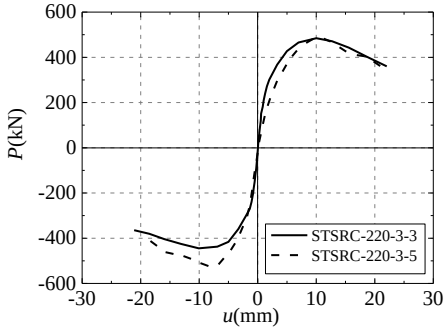

(a) Specimens with axial load ratio n = 0.3

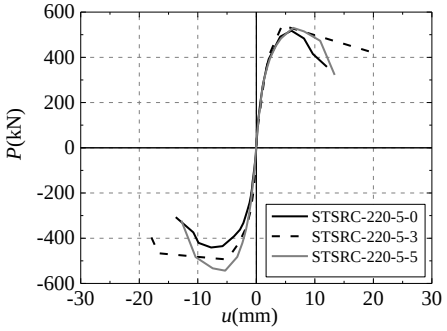

(b) Specimens with axial load ratio n = 0.5

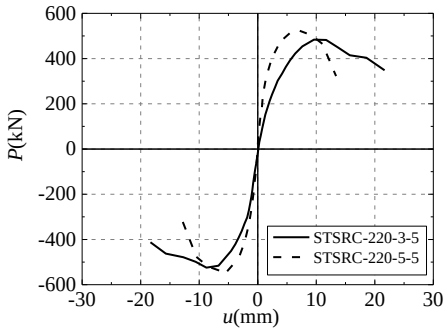

(c) Specimens with same N_s = 5 but different n

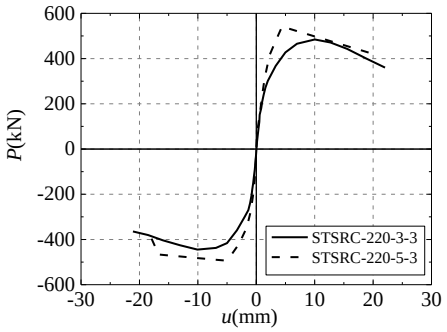

(d) Specimens with same N_s = 3 but different n

Fig. 8 Envelop curves of the specimens

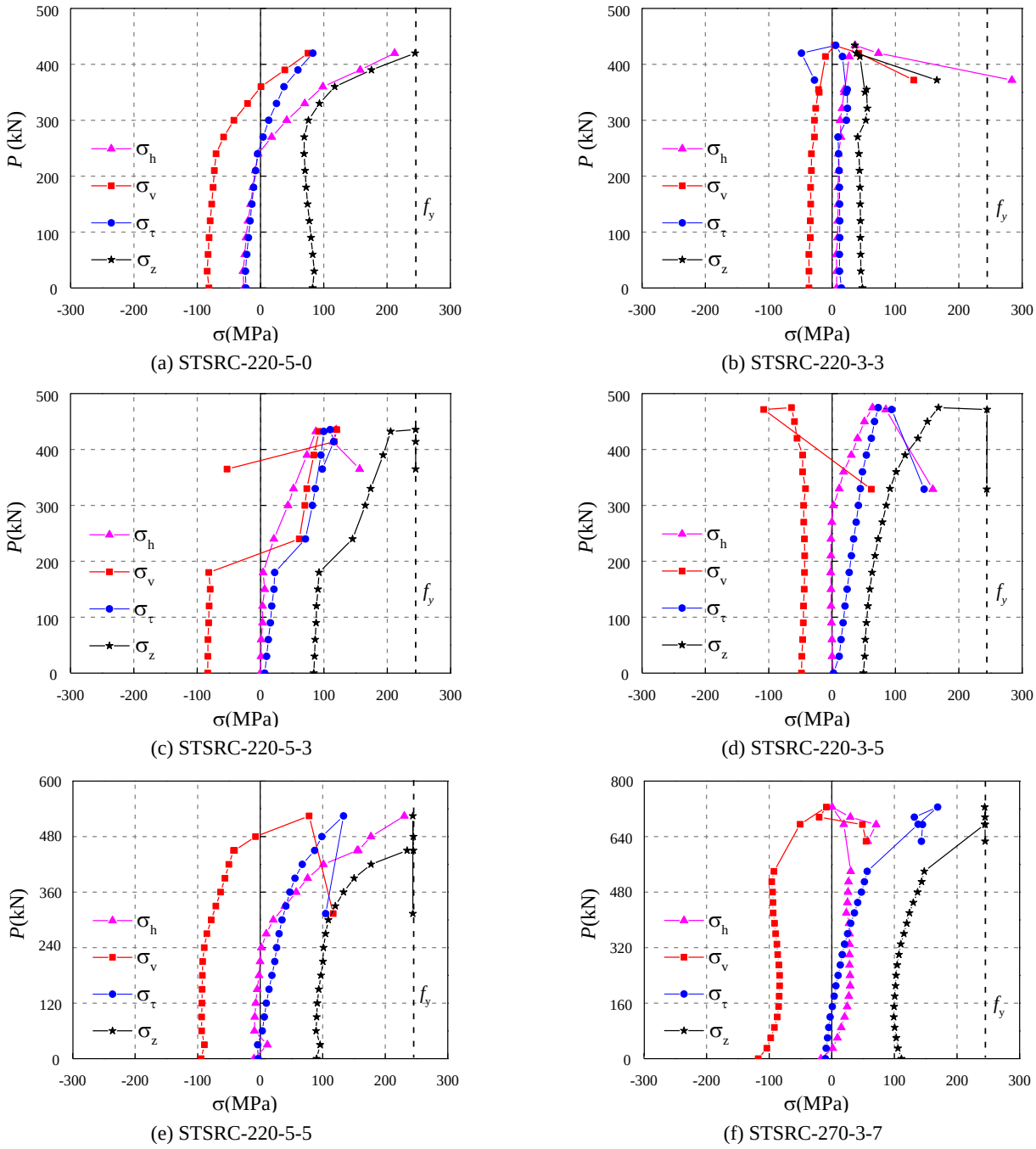

Fig. 9 Lateral load versus stress of the sheared plate of square TSRC columns

tangent stiffness of the envelop curve increased obviously in both the elastic range and the descending branch. The shear strength increases by 12.4% as the axial load ratio increased from 0.3 to 0.5, whereas φ decreases almost 22.2%. Therefore, higher axial load ratio in some degree improves the shear strength capacity of the specimen, however, the negative effect on the inelastic displacement of the column is also obvious.

3.4 Stress analysis on steel tube

The shear behavior of TSRC specimens is often directly related to the changes of strains recorded from the gauges attached to the steel tube (Zhou and Liu 2010). Fig. 9 presents the curves of lateral load P versus stresses of the sheared plate on the steel tube, where σ_v, σ_h, τ are respectively the longitudinal stress, transverse stress and shear stress, σ_z is the equivalent stress determined by

$$\sigma_z = \sqrt{\sigma_v^2 + \sigma_h^2 - \sigma_v \sigma_h + 3\tau^2} \tag{3}$$

The yield point of the steel tube was defined by Von Mises yield criterion, i.e., steel tube yielded when the equivalent stress σ_z increased to the yield strength of the steel tube f_y.

As illustrated in Fig. 9, the steel tube was generally compressed in the axial direction after completing the axial loading. It was indicated that the axial load was partially transferred from the concrete to the external steel tube due to the dilation of concrete and the friction or bond stresses between the steel tube and the concrete. The initial longitudinal stresses before applying the lateral load were significantly affected by the axial load ratio. As the axial load ratio increasing from 0.3 to 0.5, the average initial longitudinal stresses of the specimens increased from 42 MPa to 86 MPa. The transverse and shear stresses did not obviously increase until the application of lateral load. Beyond the peak lateral load, as the bond between the steel tube and the surface of concrete damaged and the transverse stresses grew rapidly, the longitudinal stresses of specimens revised from compression to tension. Besides, the shear deformation of the column resulted in a rapidly increase of the shear stress and transverse stress. Due to the outward local buckling of the steel tube in the descending branch, σ_h or τ of some specimens (i.e., STSRC-220-3-3) decreased in the descending branches and the equivalent stress σ_z therefore became lower. The equivalent stress σ_z of these specimens except STSRC-220-3-3 all arrived the yield strength of the steel tube.

3.5 Stiffness degradation

The stiffness degradation, caused by concrete cracking, outer steel tube yielding, bond slipping between steel shape and concrete, and concrete crushing, et al, is an important indicator reflecting the damage degree of the test specimens under reversed cyclic loads. In this paper, the stiffness K_i defined as the secant stiffness for a given loading cycle was used to quantify the stiffness degradation of the test specimens (Eq. (4)).

$$K_i = \frac{(|+P_i|+|-P_i|)}{(|+\Delta_i|+|-\Delta_i|)} \tag{4}$$

where $+P_i$ and $+\Delta_i$ are respectively the positive peak lateral load and displacement in the i_{th} loading cycle, $-P_i$ and $-\Delta_i$ are the negative ones.

The stiffness degradation curves of specimens with a cross-sectional side width of 220 mm are shown in Fig. 10(a). Higher axial load ratio led to higher initial stiffness, e.g., the initial stiffness of Specimen STSRC-220-5-0 with n = 0.5 is 10% higher than that of Specimen STSRC-220-3-3 with n = 0.3. Beyond the displacement corresponding to the peak lateral load, apparent degradation in stiffness is observed for the specimens with higher axial load ratio (n = 0.5). Whereas for the specimens with n = 0.3, the stiffness degradation is less rapid which results in higher plastic deformation capacity. Fig. 10(b) shows the $|K_u\text{-}K_{0.85}|/|\Delta_u\text{-}\Delta_{0.85}|$ ratios of typical specimens which can reflect the stiffness degradation in the descending branch of envelope curves, where K_u and $K_{0.85}$ are the stiffness corresponding to Δ_u and $\Delta_{0.85}$. It can be found that the increase of the axial compression ratio will significantly accelerate the degradation of the stiffness after the peak load. However, the stiffness degradation is not significant influenced by welding more shear studs on the steel shape (less than 10%).

4. Shear strength equation for short square TSRC columns

For the short square TSRC columns studied in this paper, test phenomenon indicated that the shear failure mainly happened in the middle region of the column, which belongs mainly to the B-region as compared to D-region (Fig. 11). For short frame columns with the height-to-depth ratio above 2.0, the shear strength depends on B region where the conventional beam theory was used to determine the shear strength (Collins and Mitchell 1997). According to the conventional beam theory, the nominal shear strength of short square TSRC column is contributed by concrete (V_c), steel shape ($V_{a,w}$) and outer thin-walled steel tube (V_t). Namely

$$V_n = V_c + V_{a,w} + V_t \tag{5}$$

According to the ACI 318 Code (2011), V_c for columns using HSC can be predicted from the following equation (Ou and Kurniawan 2015)

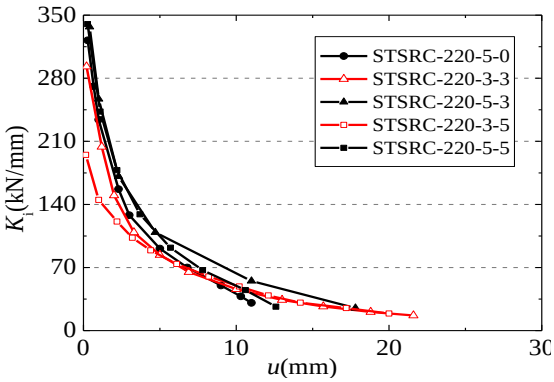

(a) K_i of specimens failed in shear mode

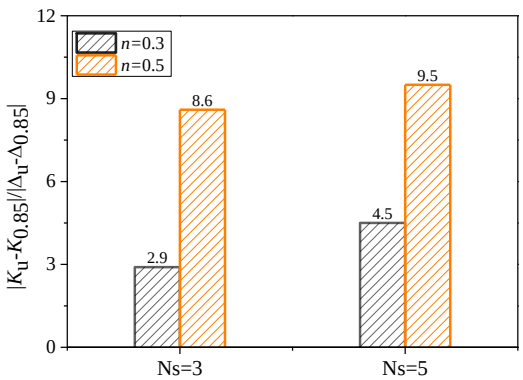

(b) $|K_u\text{-}K_{0.85}|/|\Delta_u\text{-}\Delta_{0.85}|$of specimens with shear studs

Fig. 10 Comparisons of stiffness degradation.

$$V_c = 0.25\sqrt{f_c}D^2\sqrt{1+\frac{1.6N}{\sqrt{f_c}D^2}} \quad (6)$$

For the short square TSRC columns, the inner steel shape was restricted by the concrete and the length of steel shape was relatively small. Therefore, the shear buckling of the steel shape web and the bending effect could be ignored. As such, $V_{a,w}$ was calculated without considering the shear buckling and bending effects by

$$V_{a,w} = \frac{1}{\sqrt{3}} f_{a,w} A_{a,w} \quad (7)$$

where $f_{a,w}$ is the yield strength of the steel web and $A_{a,w}$ is the area of the steel web.

For the short square TSRC columns failed in shear mode, steel tube can be equivalent to closely spaced stirrups and therefore truss analogy proposed by Ritter (1899) and Mörsch (1902) was adopted to evaluate the shear strength provided by the steel tube, as shown in Fig. 12. That is, the flexural compression concrete can be treated as the bottom chord and the steel tube in the sheared plate is acting as the web member of the truss. Therefore, V_t can be calculated by

$$V_t = 2f_{\sigma h} Dt\cot\theta \quad (8)$$

where $f_{\sigma h}$ is the transverse stress of steel tube at the peak load, taken as $0.15f_y$ which is the lower limit of the test results (Table 5), and θ is the inclined angle of the crack, taken as $\pi/6$ according to the test phenomenon.

From the above analysis, the nominal shear strength of square TSRC columns V_n can be predicted by the following equation

$$V_n = 0.25\sqrt{f_c}D^2\sqrt{1+\frac{1.6N}{\sqrt{f_c}D^2}} + \frac{1}{\sqrt{3}} f_{a,w} A_{a,w} + 0.52Dtf_y \quad (9)$$

The comparison between the predicted values using the proposed method and different experimental results from this study and other literatures (e.g., STSRC-70-X-X (Zhou and Liu 2010)), STSRC-60-X-X (Liu *et al.* 2011)) is listed in Table 5 in which only the data from the columns failing in shear are included. The comparison results indicate that the proposed equations for predicting the nominal shear strength of square TSRC columns are deemed practically acceptable.

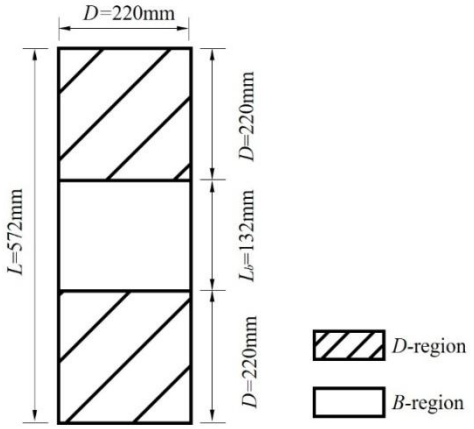

Fig. 11 B-region and D-region of test specimens with shear failure mode

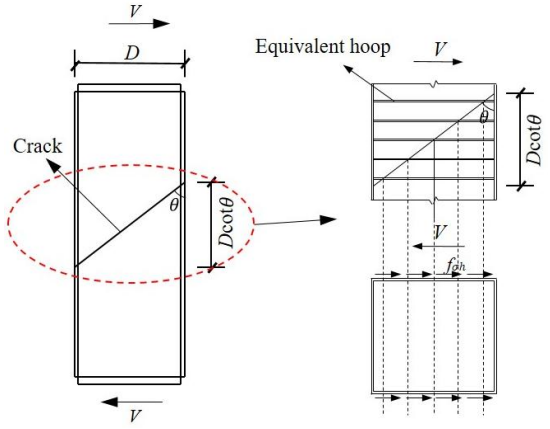

Fig. 12 The equivalent model of the steel tube

Table 5 Mechanical parameters of the specimens

Column	f_y (MPa)	$f_{\sigma h}$ (MPa)	$f_{\sigma h}/f_y$	P_u (kN)	V_n (kN)	V_n/P_u
STSRC-220-3-3	245	46.60	0.19	484.5	454.3	0.94
STSRC-220-3-5	245	63.85	0.26	483.6	454.3	0.94
STSRC-220-5-0	245	157.61	0.64	518.0	517.8	1.00
STSRC-220-5-3	245	119.38	0.49	541.0	517.8	0.96
STSRC-220-5-5	245	177.21	0.67	544.0	517.8	0.95
STSRC-70-4-1.5	254	118.39	0.47	360.2	331.6	0.92
STSRC-70-5-1.5	254	101.42	0.40	377.5	351.5	0.93
STSRC-60-2-2	309	59.04	0.19	302.7	245.2	0.81
STSRC-60-2-3	309	134.62	0.44	311.4	267.5	0.86
STSRC-60-2-4	309	207.32	0.67	369.5	287.0	0.78

5. Conclusions

In this study, six short square TSRC columns using HSC were experimentally studied. Two main parameters axial load ratio and number of shear studs on the seismic behavior of short square TSRC columns was investigated. A modified ACI design formula to predict the nominal shear strength of the adopted columns was proposed. The conclusions drawn from this study are summarized as follows.

- The tested short square TSRC columns tended to failed in combined bond and shear failure when the height-to-depth ratio was 2.6. The steel tube stiffened by diagonal plates provided effective confinement to the concrete core, resulting in generally good ductility and deformation capacity of the specimens.
- Within the parameters of this paper, the axial load played a positive role in improving the shear strength of the specimens. However, increasing the axial load ratio also resulted in a decrease in deformability and accelerated the stiffness degradation.
- Moderate difference in seismic performance between the specimens with shear studs and those without was observed. It is not recommended to use shear studs in short square TSRC columns as it failed to prevent the bond and shear failure effectively.
- An equation for predicting the nominal shear strength of short square TSRC columns was proposed based on the ACI design method, and the predictions agree well with the test results of ten specimens failed in shear from this and previous studies.

Acknowledgments

This research is made possible through the financial support from the National Key Research and Development Program of China (Grant No. 2016YFC0701201) and the National Natural Science Foundation of China (#51622802, #51438001), to which the authors are very grateful.

References

ACI 318 (2014), Building code requirements for structural concrete and commentary, American Concrete Institute; Farmington Hills, MI, USA.

An, G.H., Cha, S.L. and Kim, J.K. (2018), "Modification of the long-term deformation models for steel reinforced concrete columns", *Constr. Build. Mater.*, **189**, 245-252. https://doi.org/10.1016/j.conbuildmat.2018.08.095

CEB-FIP model code 1990 (1993), Comité Euro-International du Béton/Federation Internationale de la Precontrainte (CEB-FIP), CEB-FIP model code 1990 CEB bulletin d'Information; Thomas Telford, London, UK.

Chen, Z.P., Xu, J.J., Chen, Y.L. and Xue, J.Y. (2016), "Axial compression ratio limit values for steel reinforced concrete (SRC) special shaped columns", *Steel Compos. Struct., Int. J.*, **20**(2), 295-316. https://doi.org/10.12989/scs.2016.20.2.295

Choi, E.G., Kim, H.S. and Shin, Y.S. (2012), "Performance of fire damaged steel reinforced high strength concrete (SRHSC) columns", *Steel Compos. Struct., Int. J.*, **12**(6), 521-537. https://doi.org/10.12989/scs.2012.13.6.521

Collins, M.P. and Mitchell, D. (1997), *Prestressed Concrete Structures*, Prentice Hall Inc, Englewood Cliffs, NJ, USA.

El-Tawil, S. and Deierlein, G.G. (1999), "Strength and ductility of concrete encased composite columns", *J. Struct. Eng.*, **125**(9), 1009-1019. https://doi.org/10.1061/(ASCE)0733-9445(1999)125:9(1009)

Fam, A., Qie, F.S. and Rizkalla, S. (2004), "Concrete-filled steel tubes subjected to axial compression and lateral cyclic loads", *J. Struct. Eng.*, **130**(4), 631-640. https://doi.org/10.1061/(ASCE)0733-9445(2004)130:4(631)

Fumiya, E. and Masayuki, O. (2001), "Effects of loading rate on mechanical behavior of SRC shearwalls", *Steel Compos. Struct., Int. J.*, **1**(2), 201-212. https://doi.org/10.12989/scs.2001.1.2.201

Gardner, N.J. and Jacobson, E.R. (1967), "Structural behavior of concrete filled steel tubes", *ACI Struct. J.*, **64**(7), 404-413.

GB50010-2010 (2011), Code for design of concrete structures, Ministry of Housing and Urban-Rural Development of the People's Republic of China; Beijing, China. [In Chinese]

GB/T228-2010 (2010), GB/T228-2010 Metallic materials-Tensile resting-Part 1: Method of test at room temperature, Ministry of Housing and Urban-Rural Development of the People's Republic of China (MOHURD); Beijing, China.

Guo, L., Liu, Y., Fu, F. and Huang, H. (2019), "Behavior of axially loaded circular stainless steel tube confined concrete stub columns", *Thin-Wall. Struct.*, **139**, 66-76. https://doi.org/10.1016/j.tws.2019.02.014

Han, L.H., Yao, G.H., Chen, Z.B. and Yu, Q. (2005), "Experimental behaviours of steel tube confined concrete (STCC) columns", *Steel Compos. Struct., Int. J.*, **5**(6), 459-484. https://doi.org/10.12989/scs.2005.5.6.459

Johansson, M. and Gylltoft, K. (2002), "Mechanical behavior of circular steel–concrete composite stub columns", *J. Struct. Eng.*, **128**(8), 1073-1081. https://doi.org/10.1061/(ASCE)0733-9445(2002)128:8(1073)

Ky, V.S., Tangaramvong, S. and Thepchatri, T. (2015), "In Inelastic analysis for the post-collapse behavior of concrete encased steel composite columns under axial compression", *Steel Compos. Struct., Int. J.*, **19**(5), 1237-1258. https://doi.org/10.12989/scs.2015.19.5.1237

Liu, J.P., Abdullah, J.A. and Zhang, S.M. (2011), "Hysteretic behavior and design of square tubed reinforced and steel reinforced concrete (STRC and/or STSRC) short columns", *Thin-Wall. Struct.*, **49**(7), 874-888. https://doi.org/10.1016/j.tws.2011.02.012

Le Hoang, A., Fehling, E., Lai, B., Thai, D.K. and Van Chau, N. (2019), "Experimental study on structural performance of UHPC and UHPFRC columns confined with steel tube", *Eng. Struct.*, **187**, 457-477. https://doi.org/10.1016/j.engstruct.2019.02.063

Lu, X., Yin, X. and Jiang, H. (2014), "Experimental study on hysteretic properties of SRC columns with high steel ratio", *Steel Compos. Struct., Int. J.*, **17**(3), 287-303. https://doi.org/10.12989/scs.2014.17.3.287

McAteer, P., Bonacci, J.F. and Lachemi, M. (2004), "Composite response of high-strength concrete confined by circular steel tube", *Struct. J.*, **101**(4), 466-474.

Mörsch, E. (1902) *Der, Eisenbetonbau*: *Seine Anwendung Und Theorie*, Wayss and Freytag, AG, Im Selbstverlag der Firma, Neustadt ad Haardt.

Nematzadeh, M., Fazli, S., Naghipour, M. and Jalali, J. (2017), "Experimental study on modulus of elasticity of steel tube-confined concrete stub columns with active and passive

confinement", *Eng. Struct.*, **130**, 142-153. https://doi.org/10.1016/j.engstruct.2016.10.008
O'Shea, M.D. and Bridge, R.Q. (2000), "Design of circular thin-walled concrete filled steel tubes", *J. Struct. Eng.*, **126**(11), 1295-1303. https://doi.org/10.1061/(ASCE)0733-9445(2000)126:11(1295)
Ou, Y.C. and Kurniawan, D.P. (2015), "Shear behavior of reinforced concrete columns with high-strength steel and concrete", *ACI Struct. J.*, **112**(1), 12.
Piquer, A. and Hernández-Figueirido, D. (2016), "Protected steel columns vs partially encased columns: Fire resistance and economic considerations", *J. Constr. Steel Res.*, **124**, 47-56. https://doi.org/10.1016/j.jcsr.2016.05.011
Ritter, W. (1899), "Die bauweise hennebique", *Schweizerische Bauzeitung*, **33**(7), 59-61.
Tomii, M., Sakino, K., Xiao, Y. and Watanabe, K. (1985), "Lateral load capacity of reinforced concrete short columns confined by steel tube", *Proceedings of the International Speciality Conference on Concrete Filled Steel Tubular Structures*, Harbin, China, August.
Wang, Q., Shi, Q. and Tian, H. (2016), "Experimental study on shear capacity of SRC joints with different arrangement and sizes of cross-shaped steel in column", *Steel Compos. Struct., Int. J.*, **21**(2), 267-287. https://doi.org/10.12989/scs.2016.21.2.267
Xiong, M.X., Xiong, D.X. and Liew, J.R. (2017), "Axial performance of short concrete filled steel tubes with high-and ultra-high-strength materials", *Eng. Struct.*, **136**, 494-510. https://doi.org/10.1016/j.engstruct.2017.01.037
Xue, J.Y., Chen, Z.P., Zhao, H.T., Gao, L. and Liu, Z.Q. (2012), "Shear mechanism and bearing capacity calculation on steel reinforced concrete special-shaped columns", *Steel Compos. Struct., Int. J.*, **13**(5), 473-487. https://doi.org/10.12989/scs.2012.13.5.473
Yang, H., Liu, F. and Gardner, L. (2015), "Post-fire behaviour of slender reinforced concrete columns confined by circular steel tubes", *Thin-Wall. Struct.*, **87**, 12-29. https://doi.org/10.1016/j.tws.2014.10.014
Zhang, Y., Pei, J., Huang, Y., Lei K., Song, J. and Zhang, Q. (2018), "Seismic behaviors of ring beams joints of steel tube-reinforced concrete column structure", *Steel Compos. Struct., Int. J.*, **27**(4), 417-426. https://doi.org/10.12989/scs.2018.27.4.417
Zhao, D.Z., Wang, Q.X. and Guan, P. (2005), "Research on load-bearing capacity of steel tubular columns filled with steel-reinforced high-strength concrete subjected to compression and bending", *Ind. Constr.*, **35**(9), 84-93.
Zhao, Y.G., Lin, S., Lu, Z.H., Saito, T. and He, L. (2018), "Loading paths of confined concrete in circular concrete loaded CFT stub columns subjected to axial compression", *Eng. Struct.*, **156**, 21-31. https://doi.org/10.1016/j.engstruct.2017.11.010
Zhou, X.H. and Liu, J.P. (2010), "Seismic behavior and strength of tubed steel reinforced concrete (SRC) short columns", *J. Constr. Steel Res.*, **66**(7), 885-896. https://doi.org/10.1016/j.jcsr.2010.01.020

BU

Notation

A_c	Cross-sectional area of concrete
A_f	Cross-sectional area of flange
A_w	Cross-sectional area of web
A_g	Gross cross-sectional area
$A_{a,w}$	Area of the web of steel shape
D	Width of cross section
b_s	Flange width of steel shape
h_s	Height of steel shape section
N_s	Number of shear studs on one flange side of the steel shape
t	Wall thickness of steel tube
t_f	Thickness of steel shape flange
t_w	Thickness of steel shape web
H	Height of a specimen
N	Axial load
P	Lateral load
P_u	Peak lateral load
V_n	Nominal shear strength
V_c	Shear strength of concrete
$V_{a,w}$	Shear strength of the web of steel shape
V_t	Shear strength of steel tube
n	Axial load ratio
E_c	Elastic modulus of concrete
E_s	Elastic modulus of steel
f_c	Compressive strength of concrete
f_f	Yield strength of the flange of steel shape
f_w	Yield strength of the web of steel shape
f_y	Yield strength of steel tube
$f_{cu,150}$	Compressive strength of the 150 mm cube concrete
$f_{a,w}$	Yield strength of steel shape
$f_{\sigma,h}$	Transverse stress of steel tube at peak load
Δ_u	Lateral displacement corresponding to P_u
Δ_y	Yield displacement
$\Delta_{0.85}$	Displacement corresponding to 85% of the peak load
μ	Ductility factor
φ	Ultimate story drift ratio
θ	Crack angle